Article:
Hall, D.R., Bond, C.S., Leonard, G.A. et al. (2002) Structure of Tagatose-1,6-bisphosphate Aldolase. Insight into chiral discrimination, mechanism, and specificity of class II aldolases. Journal of Biological Chemistry, 277 (24). pp. 22018-22024. ISSN: 1083-351X

https://doi.org/10.1074/jbc.M202464200

THE JOURNAL OF BIOLOGICAL CHEMISTRY
Vol. 277, No. 24, Issue of June 14, pp. 22018–22024, 2002

Printed in U.S.A.

Structure of Tagatose-1,6-bisphosphate Aldolase

INSIGHT INTO CHIRAL DISCRIMINATION, MECHANISM, AND SPECIFICITY OF CLASS II ALDOLASES*

Received for publication, March 14, 2002, and in revised form, April 5, 2002
Published, JBC Papers in Press, April 8, 2002, DOI 10.1074/jbc.M202464200

David R. Hall‡§, Charles S. Bond‡, Gordon A. Leonard¶, C. Ian Watt‖, Alan Berry and William N. Hunter‡ ‡‡**

*From the ‡Division of Biological Chemistry and Molecular Microbiology, School of Life Sciences, University of Dundee, Dundee DD1 5EH, United Kingdom, the ¶Joint Structural Biology Group, European Synchrotron Radiation Facility, BP 220, Grenoble F38043 cedex, France, the ‖Department of Chemistry, University of Manchester, Oxford Rd., Manchester M13 9PL, United Kingdom, and the **School of Biochemistry and Molecular Biology, University of Leeds, Leeds LS2 9JT, United Kingdom*

Tagatose-1,6-bisphosphate aldolase (TBPA) is a tetrameric class II aldolase that catalyzes the reversible condensation of dihydroxyacetone phosphate with glyceraldehyde 3-phosphate to produce tagatose 1,6-bisphosphate. The high resolution (1.45 Å) crystal structure of the *Escherichia coli* enzyme, encoded by the *agaY* gene, complexed with phosphoglycolohydroxamate (PGH) has been determined. Two subunits comprise the asymmetric unit, and a crystallographic 2-fold axis generates the functional tetramer. A complex network of hydrogen bonds position side chains in the active site that is occupied by two cations. An unusual Na^+ binding site is created using a π interaction with Tyr^{183} in addition to five oxygen ligands. The catalytic Zn^{2+} is five-coordinate using three histidine nitrogens and two PGH oxygens. Comparisons of TBPA with the related fructose-1,6-bisphosphate aldolase (FBPA) identifies common features with implications for the mechanism. Because the major product of the condensation catalyzed by the enzymes differs in the chirality at a single position, models of FBPA and TBPA with their cognate bisphosphate products provide insight into chiral discrimination by these aldolases. The TBPA active site is more open on one side than FBPA, and this contributes to a less specific enzyme. The availability of more space and a wider range of aldehyde partners used by TBPA together with the highly specific nature of FBPA suggest that TBPA might be a preferred enzyme to modify for use in biotransformation chemistry.

Enzymes are valuable tools for synthetic chemistry, because, under mild conditions, they can provide both high efficiency and optical purity of products (1, 2). Recombinant DNA technology has increased the availability of useful enzymes, and technologies such as phage display and directed evolution are also being applied toward the discovery of novel bio-catalysts (3). The exciting prospect exists that, guided by structural and mechanistic understanding, we can rationally design enzyme activity for the most complex of chemical syntheses. With this long term goal in mind we have undertaken to characterize the structure-activity relationships in metal-dependent aldolases, which are particularly attractive for use in biotransformation chemistry and indeed have already contributed to the synthesis of rare sugars (4).

The most studied aldolases are the fructose-1,6-bisphosphate aldolases (FBPA),[1] which participate in two metabolic pathways. FBPA catalyzes the aldol condensation of a ketose, dihydroxyacetone phosphate (glycerone-P or DHAP), and an aldose, glyceraldehyde 3-phosphate (G3P) to form fructose 1,6-bisphosphate (FBP) in gluconeogenesis (see Fig. 1 below). In glycolysis FBPA catalyzes the reverse cleavage. FBP-aldolases are multimers of $(\alpha/\beta)_8$-barrel subunits and are divided into class I and II enzymes on the basis of mechanism. The type I enzymes utilize a lysine in Schiff base formation during catalysis and are mainly found in higher order organisms as homotetramers of molecular mass around 160 kDa (5, 6). The class II enzymes, found in yeast, bacteria, fungi, and blue-green algae, are most often dimeric and utilize a divalent metal ion, usually Zn^{2+}, in catalysis and, because they are more stable than their class I counterparts, are preferred for use in biotransformation chemistry (4, 7).

Structure-activity studies of *Escherichia coli* class II FBPA have served to delineate some details of the aldol condensation (8–14) (see Fig. 1). Of particular value is the structure of FBPA complexed to phosphoglycolohydroxamate (PGH), which mimics the ene-diolate formed from DHAP (15), the EH·DHAP(C^-) structure (*stage II* in Fig. 1). Two critical steps in the aldol condensation are: first, the formation of an activated carbon from which a proton is abstracted to produce an enolate and, second, the formation of a new C–C bond. During catalysis, direct coordination of DHAP to Zn^{2+} aligns the substrate allowing the divalent cation to function as a Lewis acid and to polarize the carbonyl bond of the ketose ready for a reaction that involves three major covalency changes (see Fig. 1). The first covalency change follows abstraction of the *1-proS* proton of DHAP to produce the ene-diolate, the second is carbon–carbon bond formation to covalently link DHAP C1 with G3P C1 and so form the new C3–C4 bond of a hexose bisphosphate.

* This work was supported by the Wellcome Trust and the Biotechnology and Biological Sciences and Research Council (United Kingdom). The costs of publication of this article were defrayed in part by the payment of page charges. This article must therefore be hereby marked "*advertisement*" in accordance with 18 U.S.C. Section 1734 solely to indicate this fact.

The atomic coordinates and structure factors (code 1GVF and R1GVFSF) have been deposited in the Protein Data Bank, Research Collaboratory for Structural Bioinformatics, Rutgers University, New Brunswick, NJ (http://www.rcsb.org/).

§ Current address: Molecular Enzymology Group, Cancer Research UK, Clare Hall, Potters Bar, South Mimms EN6 3LD, United Kingdom.

‡‡ To whom correspondence should be addressed. Tel.: 44-1-382-345-745; Fax: 44-1-382-345-764; E-mail: w.n.hunter@dundee.ac.uk.

[1] The abbreviations used are: FBPA, fructose-1,6-bisphosphate aldolase; DHAP, dihydroxyacetone phosphate; G3P, glyceraldehyde 3-phosphate; FBP, fructose 1,6-bisphosphate; PGH, phosphoglycolohydroxamate; EH, protonated enzyme; TBPA, tagatose-1,6-bisphosphate aldolase; TBP, tagatose 1,6-bisphosphate; MAD, multiwavelength anomalous dispersion; r.m.s.d., root mean square deviation.

The substrate oxygen ligands are *syn* to the enolate bond, and this restricts access of the electrophilic G3P to the *Si* face of DHAP as the C3–C4 bond is formed. In the third covalency change, a second proton transfer converts the C4 carbonyl to a hydroxyl group and so completes the hexose synthesis.

Despite some progress in understanding class II aldolases, there remain aspects of aldolase reactivity that require clarification. We have carried out studies on tagatose-1,6-bisphosphate aldolase (TBPA), a tetrameric enzyme that catalyzes the condensation of DHAP with the natural substrate G3P to form tagatose 1,6-bisphosphate (TBP) (9, 16) a diastereoisomer of FBP (Fig. 1). The reactions catalyzed by TBPA and FBPA (Fig. 1) are similar, and because there is significant conservation of sequence (9) and structure (this work) a comparison provides insight into class II aldolase mechanism and specificity. The major products of the condensations catalyzed by TBPA and FBPA are distinct in their chirality at C4 (Fig. 1). On the basis of k_{cat}/K_m values, FBPA prefers FBP around 1500-fold over TBP so that the overall discrimination between the two substrates is nearly 5×10^5 (9). FBPA and TBPA, therefore, represent an excellent model system to investigate the molecular basis of chiral discrimination.

We now report the high resolution crystal structure of recombinant *E. coli* TBPA, which encoded by the *agaY* gene and complexed to PGH, and a detailed comparison with the structure of recombinant *E. coli* FBPA also complexed with PGH (8). Although, to date, we have been unable to obtain crystal structures of complexes with a hexose substrate or analogue, we have carried out modeling to generate templates for the TBPA·TBP and FBPA·FBP complexes based on the experimentally derived structures.

EXPERIMENTAL PROCEDURES

Crystallization, Data Collection, and Processing—Established protocols provided the enzyme (9) and PGH (8, 15). The enzyme (6.5 mg ml^{-1} in 50 mM Tris-HCl, pH 7.5) was incubated for 1 h at 4 °C with 20 mM PGH and crystallization achieved in hanging drops of 5 μl of enzyme·PGH complex mixed with 5 μl of reservoir comprising 7–12% (v/v) ethylene glycol, 10 mM $ZnCl_2$, 42 mM sodium cacodylate, pH 6.4. Orthorhombic crystals attained dimensions of $0.20 \times 0.25 \times 0.30$ mm after 3 weeks at 20 °C. The space group is I222 with unit cell lengths of $a = 72.6$, $b = 100.5$, $c = 206.7$ Å and two TBPA subunits per asymmetric unit. All diffraction measurements were carried out on crystals cryoprotected with ethylene glycol and cooled to −173 °C in a stream of nitrogen gas.

Data were first measured in-house using a Rigaku rotating anode (CuK_α) and RAXIS IV image plate detector, then at European Synchrotron Radiation Facility stations BM14 and ID14-EH2, for a four-wavelength MAD experiment and the high resolution data, respectively, using MAR charge-coupled device detectors. Wavelengths for the MAD experiment (peak λ_1, inflection point λ_2, and remote data λ_3, λ_4) were derived from an x-ray near edge absorption scan (XANES) of the zinc K-edge and selected to maximize the anomalous differences, f'' (λ_1), provide the minimum f′ (λ_2), and two remote wavelengths (λ_3, λ_4) to maximize dispersive differences ($\lambda_3 - \lambda_2$, $\lambda_4 - \lambda_2$). All data were processed using HKL (17). The in-house and high resolution data were scaled together to improve the low resolution terms, and this combined data set was used for refinement (Table I).

MAD Phasing, Model Building, and Refinement—Two Zn^{2+} positions, identified from an anomalous difference Patterson synthesis, were used to phase the λ_2 data to 2.2 Å with a figure-of-merit of 0.54 (18). Solvent flattening and histogram matching (19, 20) followed and raised the overall figure-of-merit to 0.82. Phasing statistics are presented in Table I.

Automated procedures (21, 22) constructed ~85% of residues for the two subunits in the asymmetric unit and further rounds of model

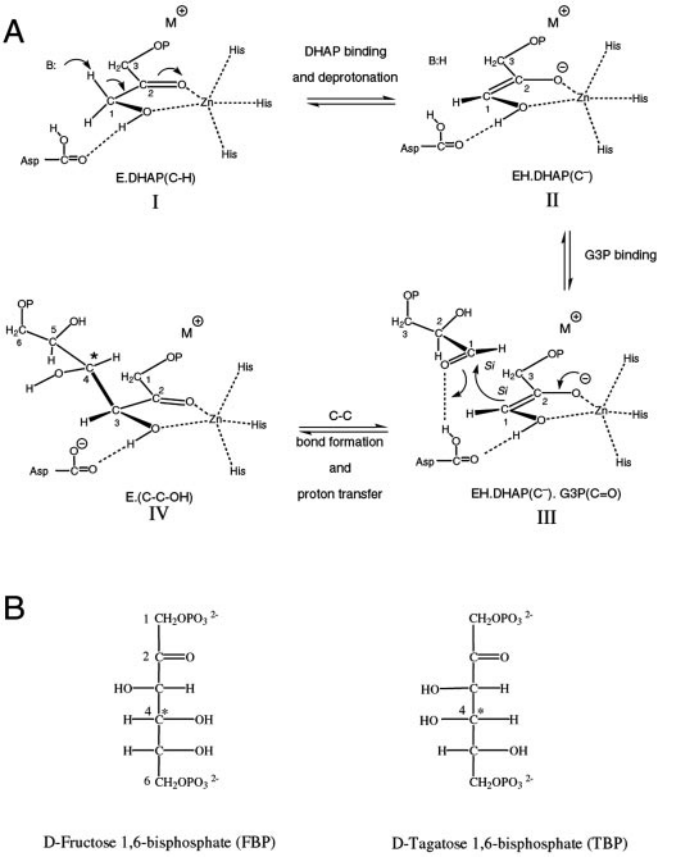

FIG. 1. *A*, the condensation mechanism of the reaction catalyzed by fructose-1,6-bisphosphate aldolase (FBPA) and tagatose-1,6-bisphosphate aldolase (TBPA), respectively. Each of the four distinct states is discussed in the text. *B*, a functional group able to abstract a proton from the activated C1; M_+, a monovalent cation. The aspartate corresponds to Asp^{109} in FBPA, Asp^{82} in TBPA. The *asterisk* in stage IV marks C4, the chiral center which distinguishes (*B*) D-fructose 1,6-bisphosphate (*left*) and D-tagatose 1,6-bisphosphate (*right*).

TABLE I
Data and phasing statistics

	λ_1 (peak)	λ_2 (inflection)	λ_3 (remote)	λ_4 (remote)	Combined in-house/ESRF
Wavelength (Å)	1.2820	1.2830	1.1270	1.030	1.5418/0.9330
Resolution range	29.9 –2.20	24.5 –2.20	24.5 –2.20	24.5 –1.90	29.8 –1.45
Measurements	127,103	127,046	177,731	204,335	1,086,028
Unique reflections	37,051	37,085	54,207	60,423	131,455
Coverage overall	93.8	93.8	89.0	85.1	98.4
R_{sym} (%)[a]	3.2 (11.9)[b]	3.4 (14.5)	4.6 (28.0)	4.1 (34.8)	6.4 (29.2)
R_{anom} (%)[c]	3.7 (9.3)	2.9 (9.9)	4.5 (23.9)	3.8 (28.4)	
Phasing power[d]					
Accentric/centric	0.75/0.62		0.78/0.87	1.19/0.79	

[a] $R_{sym} = \Sigma|I - \langle I\rangle|/\Sigma I$, where the summation is over all symmetry equivalent reflections.
[b] *Numbers in parentheses* refer to a high resolution bin of approximate width 0.1 Å.
[c] $R_{anom} = \Sigma|I(+) - I(-)|/\Sigma(I(+)-I(-))$.
[d] Phasing power is the root-mean-square ($|F_H|/E$), where F_H is the calculated heavy-atom structure factor from two Zn^{2+} positions and E is the residual lack of closure.

TABLE II
Refinement and model geometry statistics

Protein residues/atoms	548/4259
PGH atoms/ions/solvents	20/2 Zn^{2+}, 2 Na^{+}/658 waters, 14 ethylene glycols
R-work/No. of observations	0.13/124,490
R-free/No. of observations	0.17/6,592
Wilson *B* ($Å^2$)	16.2
Average isotropic thermal parameters ($Å^2$)	
Subunit A/B overall	18.0/20.6
Main chain/side chain	16.4/22.4
Solvents/PGH/ethylene glycol	35.2/17.5/43.4
Residues in dual conformations[a]	134A, S39A, R42A, I57A, R91A, V98A, E159A, K7B, I57B, R91B, V98B, R162B, R198B, R272B, V277B
Residues for which there is no convincing electron density at the side chain[a]	S151A, K185A, K188A, R257A, S285A, E150B, S151B, K185B, K188B, E216B
r.m.s. bond lengths (Å)	0.018
r.m.s. bond angle associated distances (Å)	0.030
r.m.s. planarity (Å)	0.025

[a] The single-letter amino acid code, the residue number, and subunit assignment A or B.

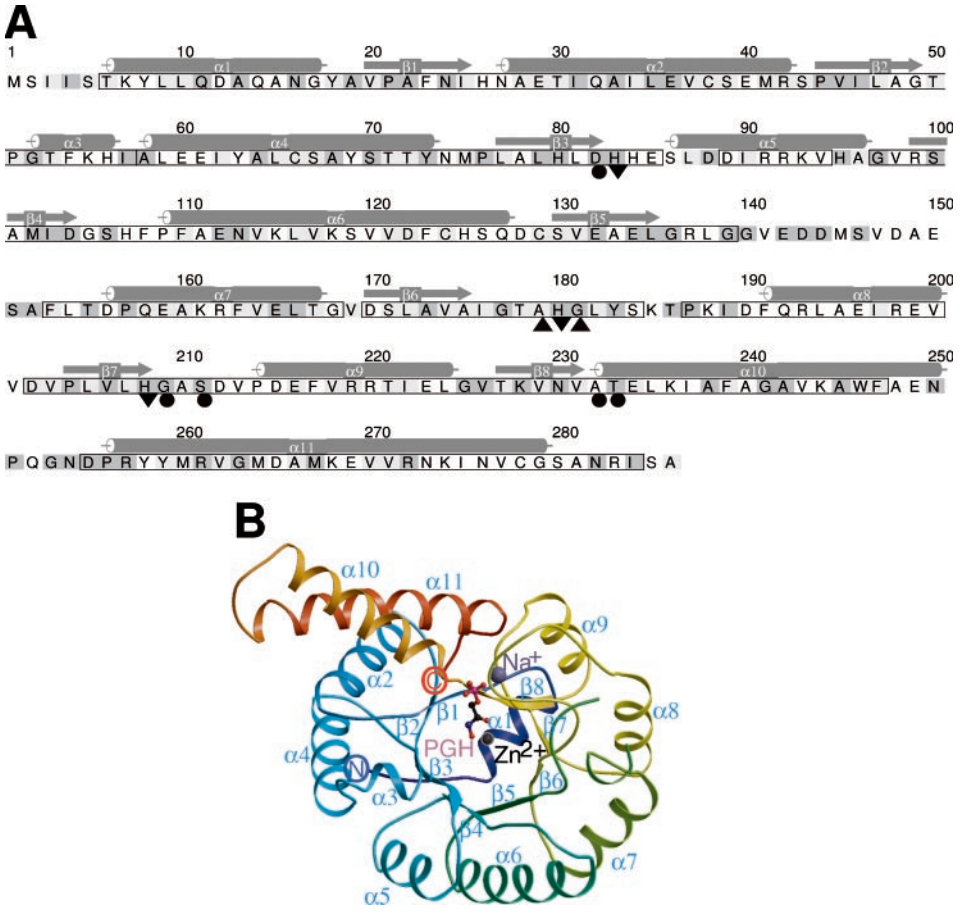

FIG. 2. **The sequence and structure of *E. coli* TBPA.** *A*, amino acid sequence and secondary structure assignment. *Cylinders* depict α-helices, *arrows* are β-strands. *Shaded residues* are conserved in *E. coli* FBPA. This image was created using ALSCRIPT (33). *B*, ribbon diagram of a subunit with PGH shown as a *ball-and-stick model* colored according to atom type, nitrogen (*cyan*), carbon (*black*), oxygen (*red*), and phosphorus (*pink*). N- and C-terminal positions are marked, and the cations are depicted as *spheres*, *blue* for Na^{+}, *black* for Zn^{2+}.

building, map interpretation (23), and refinement (22) improved this model. It was then refined using the 1.45-Å data set first with rigid body refinement to account for the lack of isomorphism (R_{iso} 0.26) with the MAD data set. Restrained anisotropic refinement without noncrystallographic symmetry restraints was implemented first with CNS (24) then completed using SHELXL with riding hydrogens (25, Table II). The final model consists of residues 2–139 and 151–285 of subunit A and 2–141 and 150–284 of subunit B, two Zn^{2+} ions, two Na^{+} ions, 658 waters, and 14 ethylene glycol molecules. Fifteen side chains were modeled in dual conformations, and ten, with poorly defined electron density, were given zero occupancy. There are no Ramachandran outliers, and further details are presented in Table II. The structure and interactions with ligands are well conserved among the two subunits, for example, the 272 Cα atoms common to each overlay with an root mean square deviation of 0.31 Å, and it is therefore appropriate to only detail one active site.

Molecular Modeling—Molecular docking experiments were performed using AutoDock version 3.0.3 (26) and GRID (27). Receptor models for TBP aldolase and FBP aldolase were derived from the complexes with PGH with all water molecules removed. In addition, for FBPA the side chain of Glu^{182} was deleted to allow access to Arg^{331}, which has been shown to interact with the G3P phosphate of the substrate (12) and to be consistent with TBPA for which the corresponding residue Glu^{142} is disordered and missing from the model. Suitable parameters for the Zn^{2+}, Na^{+}, and substrate atoms were derived by reference to literature values (28) and systematic variation to reproduce the position of PGH observed in the experimentally derived crystal structures. Coordinates for the hexose substrates were prepared using

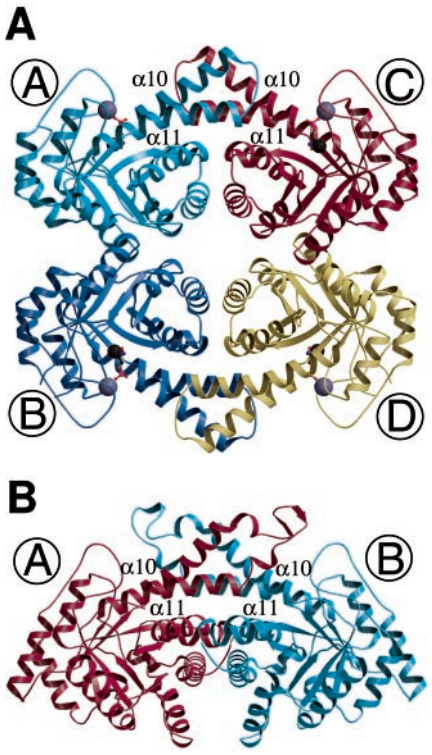

FIG. 3. *A*, the functional TBPA tetramer with each subunit given a *different color* and labeled *A* to *D*. PGH and cations are included as in Fig. 2. The orientation of the subunit shown in Fig. 2 is approximately perpendicular to subunit C in this figure. *B*, the functional FBPA dimer with subunits A and B in similar orientation to the TBPA subunits A and C. The helices α10 and α11, important for oligomerization, are labeled for both enzymes. Figs. 3–5 were generated using MOLSCRIPT (34) and RASTER-3D (35).

Chem3D (CambridgeSoft) and PRODRG (29). The 2–3 bonds (Fig. 1) were fixed, and torsional freedom was allowed in all other 11 torsion angles. Consistent results were achieved using the genetic algorithm with 40 trials and a maximum of 1400 generations.

RESULTS AND DISCUSSION

Architecture of the Subunit and Functional Tetramer—The TBPA subunit comprises 285 residues folded into an $(\alpha/\beta)_8$ barrel carrying three additional helical segments. The secondary structure is mapped onto the amino acid sequence and the three-dimensional arrangement shown in Fig. 2. The elements of secondary structure that create the barrel are β1-α2-β2-α4-β3-α5-β4-α6-β5-α7-β6-α8-β7-α9-β8-α10. Helix α1 caps the N-terminal section of the barrel, and α3 comprises two turns of helix linking β2 with α4. Helix α11 is closely associated with α10 and together with the intervening loop forms an "arm" protruding away from the barrel (Figs. 2*B* and 3*A*), which provides an important component for subunit·subunit interactions.

The TBPA and FBPA monomers have similar dimensions (Fig. 3), but a noteworthy difference is that the α10-loop-α11 arm is ~12 Å shorter in the former. On the basis of a structural alignment the *E. coli* class II FBPA and the *agaY*-encoded TBPA enzymes share ~23% sequence identity (Fig. 2) and 268 Cα atoms from each subunit overlay with an r.m.s.d of 1.56 Å (not shown). However, the quaternary structure differs between the dimeric FBPA and the tetrameric TBPA. The functional TBPA tetramer (subunits A, B, C, and D arranged with 222 point group symmetry) is a rectangular block with approximate dimensions of 92 × 85 × 38 Å (Fig. 3*A*).

The A-B and A-C associations represent two distinct subunit-subunit interfaces. The A-B interface involves the interaction of residues at the N-terminal region of α1 with the turn linking α6 and β5 of an adjacent subunit, resulting in the N-terminal portion of the two $(\alpha/\beta)_8$ barrels abutting each other in the dimer and the point group symmetry positioning an active site at each corner of the rectangular-shaped tetramer.

The two subunits of the TBPA asymmetric unit (A and B) give an arrangement distinct from that observed for functional FBPA. Rather it is the combination of TBPA subunits A and C (or B and D) that forms a dimer similar to FBPA (Fig. 3). This interaction between subunits A and C covers a larger area than the other type of interface (A-B) and is essential to complete the TBPA active site. The A-C interface is formed by the antiparallel alignment of helices α4 together with interactions from residues at the C-terminal region of the short α3 helix with residues on helices α2 and α4 of the partner subunit. Of particular note is the packing of hydrophobic residues carried on one α10-loop-α11 arm with that of the partner subunit in a manner similar to that observed in FBPA, although this loop is truncated by ~12 residues in TBPA. Dimer formation by subunits A and C directs the side chain of Arg^{257} into the active site of the partner subunit in similar fashion to that observed for the C6P binding residue, Arg^{331} of FBPA (13).

The Active Site of TBPA and Interactions with PGH—The catalytic center is located in a deep, polar cavity at the C-terminal end of the $(\alpha/\beta)_8$-barrel (Fig. 4), and a complex network of hydrogen bonds organize the positions of key functional groups and metal ion ligands. The active site can be divided into a monovalent cation binding site, a divalent cation binding site, the PGH (DHAP) binding site, and the G3P site.

TBPA has, like FBPA, a well-defined monovalent cation (Na^+) binding site, ~8.5 Å from the catalytic Zn^{2+}, which serves to create a phosphate binding site and tethers PGH, and by inference the natural substrate DHAP, in the active site. The Na^+ coordinates the carbonyl oxygens of four residues (Ala^{179}, Gly^{181}, Gly^{209}, and Ser^{211}) together with a PGH phosphate oxygen. The Na^+ O distances fall in the range 2.3–2.6 Å. In FBPA the octahedral Na^+ coordination sphere is completed by a water, but in TBPA an uncommon π-cation interaction involving the side chain of Tyr^{183} is observed (Fig. 4). A similar π-cation interaction involving a Na^+·tryptophan association has been observed in lysozyme (30), but such a mode of metal binding has, to the best of our knowledge, not been observed before in an enzyme active site. Although the sequence of *E. coli* FBPA carries a tyrosine (Tyr^{229}) at the same place in the structure as Tyr^{183} in TBPA, it adopts a different orientation at the surface of FBPA. The differences observed in the FBPA main chain are due to interactions with the extremity of the partner subunit α10-loop-α11 arm, interactions that are absent in TBPA because the arm is truncated as described earlier. The Na^+ binding site in TBPA is important for the formation of the PGH/DHAP phosphate binding site and in addition helps to position His^{180} to coordinate the catalytic Zn^{2+}.

The PGH phosphate binds in a site created by strands β7, β8, the loop linking β6 with α8, and the N-terminal region of α10. The latter provides a helix dipole to assist phosphate binding whereas the β8 strand runs close to the inhibitor and imposes steric restrictions at the methylene group of PGH, and by implication C3 on DHAP. In addition to the direct coordination to Na^+, the phosphate has two bifurcated hydrogen bond interactions with the main chain amides of Gly^{181} and Thr^{233}, single hydrogen bonds accepted from the amides of Ser^{211} and Ala^{232}, the side chain hydroxyls of Ser^{211} and Thr^{233} (Fig. 4), and with a water (not shown).

The PGH enolate (O1) and hydroxyl (O2) groups chelate the catalytic Zn^{2+}, and a trigonal bipyramidal coordination sphere is completed by three histidines (His^{83} Nε2, His^{180} Nε2, and His^{208} Nδ1, Fig. 4). The metal-ligand distances fall in the range

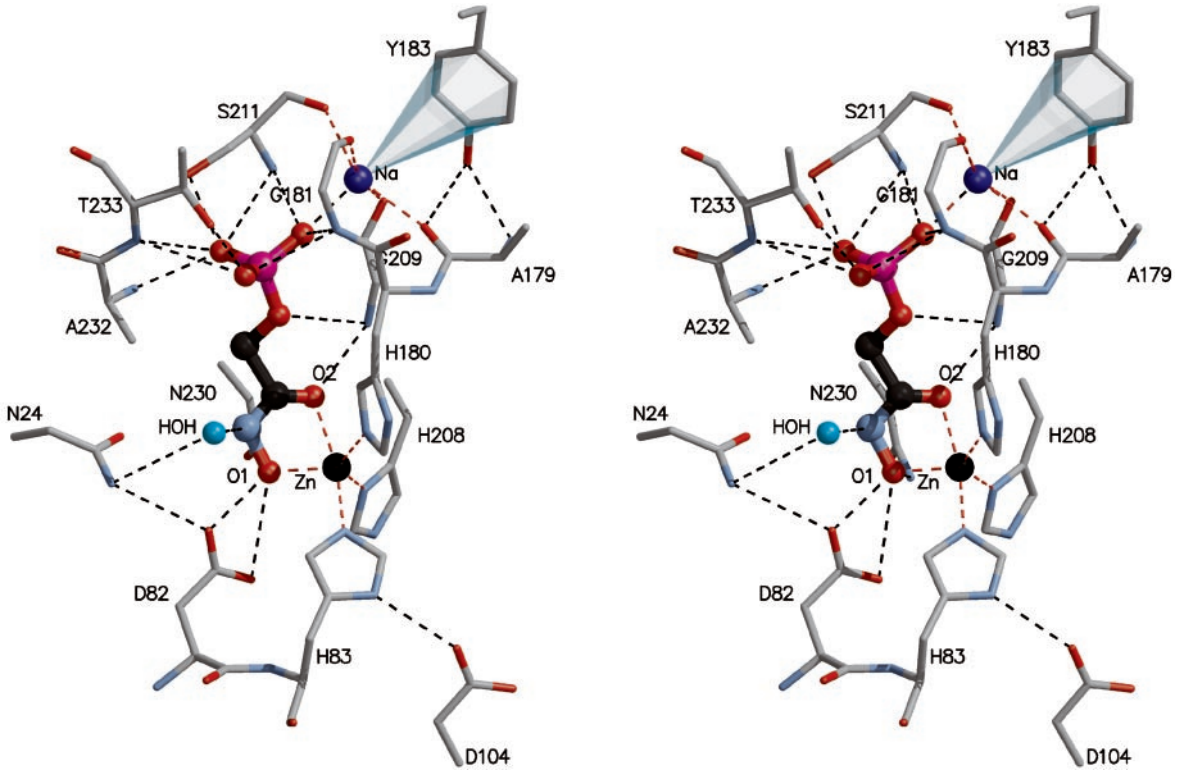

FIG. 4. **PGH interactions in the active sites of TBPA.** *Dashed lines* represent potential hydrogen bonds (*black*) or metal ion ligand interactions (*red*). Amino acid side chains are colored, *gray* for carbon, *light blue* for nitrogen, and *red* for oxygen. The *green sphere* represents a water molecule in the active site, and the *blue shading* represents interactions between Na^+ and Tyr^{183}.

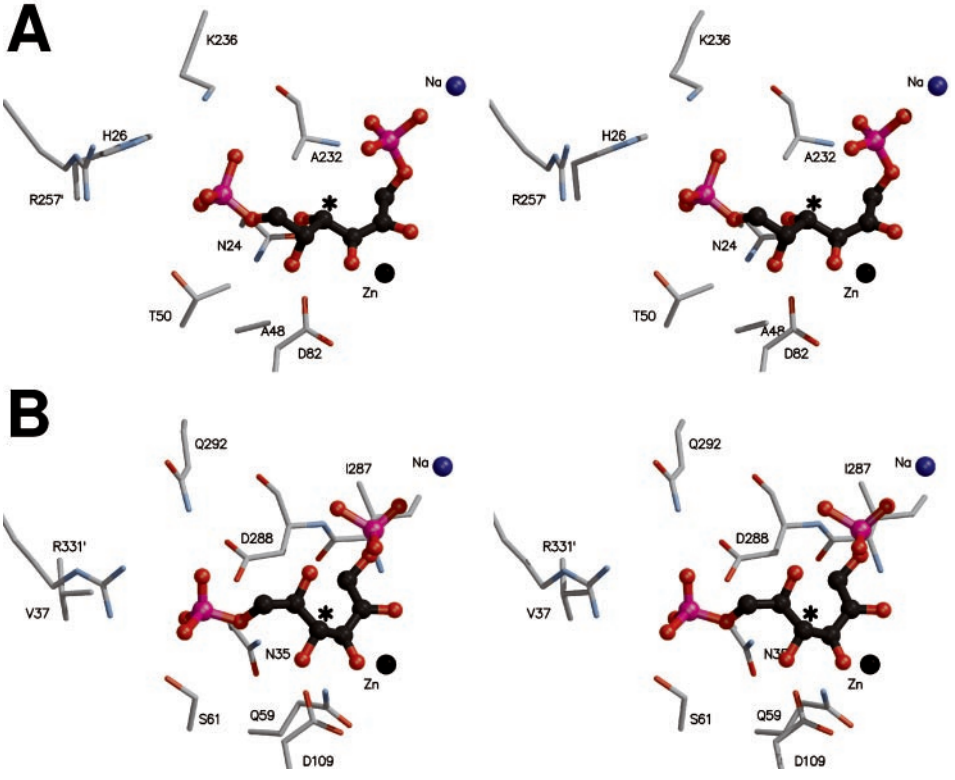

FIG. 5. **Models of the enzyme hexose substrates/product complexes.** *A*, TBP in the active site of TBPA; *B*, FBP in the active site of FBPA. The same color scheme as used in other figures applies here. An *asterisk* is used to highlight the C4 position, and the chirality at this position distinguishes TBP from FBP.

2.0–2.4 Å. The Zn^{2+} binding site is well-ordered by a complex network of hydrogen bonding interactions. His^{83} and His^{208} are held in place by hydrogen bonds donated to the side chain of Asp^{104} and Glu^{132} (not shown), respectively. Glu^{132} also participates in a buried salt bridge with Lys^{228}, which in turn hydrogen bonds to and orients the side chain of Asn^{230}. The side

chain of Asn^{230} forms part of the active site floor and donates a weak hydrogen bond of length 3.3 Å to PGH O4. Asn^{230} is structurally conserved and corresponds to Asn^{286} in FBPA. In both enzymes the amino group is positioned just under the substrate analogue and serves both to restrict the stereospecificity of the catalytic reaction at DHAP C1 and to assist carbanion formation during catalysis (8). An asparagine at this position is critical for FBPA, because site-directed mutagenesis of Asn^{286} to aspartate or alanine greatly reduces k_{cat} by up to 8000-fold (10).

PGH O1, in addition to coordinating Zn^{2+}, accepts a hydrogen bond from the amide of Gly^{209} while PGH O_2 donates a hydrogen bond to the carboxylate group of Asp^{82}. At this point we note that the residue types and their interactions with each other as described above are conserved between FBPA and TBPA. This strongly implies a conservation of substrate recognition between FBPA and TBPA for DHAP and the enzyme mechanism.

Both TBPA and FBPA require deprotonation of DHAP and carbanion formation to produce the unsaturated linkage where the aldol condensation occurs (Fig. 1). There are only a few residues in the active sites that provide a basic group to abstract the acidic *1-proS* α-H. In FBPA these are Glu^{182}, Asp^{109}, Asp^{288}, and then Asp^{329} from the partner subunit. Site-directed mutagenesis experiments indicate that the aspartates do not abstract the proton from DHAP and implied that Glu^{182} could be responsible (10). Subsequent mutagenesis of Glu^{182} to alanine and kinetic analysis of the altered protein showed that proton abstraction became rate-limiting, clearly identifying a role in deprotonation (14). Glu^{182} is positioned on a flexible loop (8) about 6.8 Å from the PGH N2 and a conformational alteration would be required to position the side chain where direct abstraction of a proton from DHAP C1 would be feasible.

Glu^{182} of FBPA corresponds to Glu^{142} in TBPA, which is also positioned on a glycine-rich loop. Due to the lack of reliable electron density, this residue has not been included in the TBPA model and it is presumed to be flexible and disordered. The sequence conservation of this loop in TBPA and FBPA is high (Fig. 2), which implies that Glu^{142} could adopt a similar position and contribute the same function as Glu^{182} in FBPA. We would therefore predict that mutagenesis of Glu^{142} in TBPA would have the same effect as seen for Glu^{182} in FBPA.

An alternative hypothesis, which would still involve Glu^{182}/Glu^{142}, to explain proton abstraction from DHAP C1 involves the use of activated water. In both the FBPA and TBPA·PGH complex structures there is a well-defined water molecule within hydrogen bonding distance of the PGH N2 and correctly positioned to interact with the *1-proS* α-H of these class II aldolase·DHAP complexes (Fig. 4). This water therefore represents a potential base for the proton abstraction. In FBPA and TBPA the water is hydrogen bonded to other solvents in the active site and in the former a hydrogen bond network extends up to Glu^{182} (8). In the absence of PGH the catalytic Zn^{2+} of FBPA is five-coordinate, using three histidines and two water molecules (11). The water ligands are replaced by PGH and, by implication, DHAP during catalysis (8). The replacement of such cation-binding solvent by hydroxamates is common to other zinc enzyme inhibitor complexes (31) and a possibility is that the Zn^{2+} contributes to activating a water. We note that details of a similar proton abstraction step in class I aldolases has proven difficult to explain. However, the recent work of Heine *et al.* (32) has indicated that for D-2-deoxyribose-5-phosphate aldolase a proton relay system activates an active site water, which then mediates proton transfer. Our analysis does not unambiguously explain the details of proton abstraction in the class II aldolase system but does suggest that the potential role of activated water should be investigated.

The Structural Basis of Chiral Discrimination—The major differences between the TBPA and FBPA active sites are localized to that region where G3P has to bind, and, although the main chain of the enzymes overlay well, we note two sequence changes that alter side chain contributions to the active sites (Fig. 5). Gln^{59} and Asp^{288} of FBPA correspond to Ala^{48} and Ala^{232}, respectively, in TBPA. This results in more space on one side of the TBPA active site and influences the side-chain orientation of a conserved asparagine (Asn^{35} in FBPA; Asn^{24} in TBPA). The asparagine Nδ2 groups are structurally conserved when the TBPA and FBPA models are overlaid (not shown) as is the hydrogen bond formed with another conserved residue: Asp^{109} in FBPA and Asp^{82} in TBPA. In FBPA, Asn^{35} Oδ1 is held in place by accepting a hydrogen bond from Gln^{59} Nϵ2 whereas Asn^{35} Nδ2 donates a hydrogen bond to Asp^{288}. In TBPA, however, the loss of functional groups and side-chain atoms results in more space in the TBPA active site. The side chain of TBPA Asn^{24} adopts a different conformer, and the Oδ1 group alters position with respect to that seen in FBPA. The result is that, although Nδ2 of Asn^{35} FBPA and Asn^{25} TBPA occupy the same relative position, the Oδ1 groups occupy different locations in the active site.

The complexes with PGH mimic the ene-diolate enzyme structures (stages I through II in Fig. 1) formed from DHAP. We previously modeled the other reactant, G3P into the active site of FBPA on the basis of simple graphical considerations (stage III, 8) but have now used computational chemistry methods to position FBP and TBP in the active sites of their cognate enzymes, in effect to model stage IV (Fig. 1) for each aldolase. Although crude, these models serve to identify possible interactions of relevance to enzyme mechanism and specificity.

The lowest energy FBP models in the active site of FBPA, of which one is shown in Fig. 4, placed the C6 phosphate to interact with Arg^{331} of the partner subunit and Ser^{61}. These residues are conserved in the class II FBP-aldolases, and the model is consistent with the kinetic analysis of mutant enzymes in which these two residues have been altered (9, 12). The C4 hydroxyl of FBP is positioned about 4 Å from Asn^{35} and 3 Å from the carboxylate side chain of Asp^{109}. Mutagenesis of the asparagine in FBPA to alanine produced an enzyme with ~1.5% of the activity of wild-type protein (9), and the FBPA·FBP model suggests a role in binding the C4 OH. Asp^{109} has previously been shown to be responsible for the protonation of the incoming C4 carbonyl group (Fig. 1, stage III, 10).

The docking of TBP into the active site of TBPA did not produce a set of closely clustered models as observed for the FBPA·FBP combination but indicated that a range of conformations of the G3P component are accessible. This suggests that the TBPA active site allows the substrate more conformational freedom than is the case for FBPA. We present one of the TBP·TBPA models in Fig. 5, which, like the others, suggests that the G3P phosphate interacts with a basic patch, including His^{26}, Lys^{236}, and from the partner subunit Arg^{257}, which corresponds to Arg^{331} in FBPA discussed above. In addition the phosphate is placed near Thr^{50}, which corresponds to Ser^{61} in FBPA. His^{26} and Lys^{236} are altered in FBPA to Val^{37} and Gln^{292}, respectively (Fig. 5). The C4 OH group of TBP is directed into the space between the side chains of Ala^{232} and Asp^{82} and in position to interact with Asn^{24}. Asp^{82} corresponds to Asp^{109} in FBPA and, by analogy with FBPA, we judge it likely that this residue is responsible for the protonation of the C4 carbonyl of during the aldol condensation to produce TBP.

An overlap of both enzyme active sites and substrate models (not shown) suggests that there would be a significant steric clash between the G3P of TBP with Asp^{288} of FBPA in addition

to the electrostatic repulsion of anionic groups. Such interactions are likely a contributory discriminating factor in the specificity of FBPA. Superposition of FBP models in the active site of TBPA does not predict any major steric clash.

In contrast to FBPA, TBPA displays poor stereochemical control with nearly 10% of the L-*erythro* configuration being observed and about 90% of the D-*threo*. In addition, TBPA can utilize glycoaldehyde, L-glyceraldehyde, acetaldehyde, and isobutyraldehyde as the DHAP partner (16). This lack of specificity can be explained by the availability of space in that part of the active site where the aldehyde binds. It appears that FBPA has an active site that is complementary to and highly specific for its cognate substrates. TBPA on the other hand is less specific due to the conformational freedom afforded its range of substrates. We conclude that the overall discrimination between the two systems is dominated by the strict specificity of FBPA, and, therefore, TBPA might be the better choice of enzyme to serve as the framework onto which new catalytic activities could be constructed.

Acknowledgments—We thank European Synchrotron Radiation Facility for access and our colleagues for encouragement and excellent support in particular Drs. Graeme Thomson and Shaza Zgiby for help in the preparation of enzyme.

REFERENCES

1. Takayama, S., McGarvey, G. J., and Wong, C.-H. (1997) *Annu. Rev. Microbiol.* **51,** 285–310
2. Wong, C.-H., and Whitesides, G. M. (1995) *Enzymes in Organic Synthesis. Tetrahedron Organic Chemistry Series Volume 12*, Pergamon Press, New York
3. Marrs, B., Delagrave, S., and Murphy, D. (1999) *Curr. Opin. Microbiol.* **2,** 241–245
4. von der Osten, C. H., Sinskey, A. J., Barbas, C. F., Pederson, R. L., Wang, Y.-F., and Wong, C.-H. (1989) *J. Am. Chem. Soc.* **111,** 3924–3927
5. Gefflaut, T., Blonski, C., Perie, J., and Willson, M. (1995) *Prog. Biophys. Mol. Biol.* **63,** 301–340
6. Blom, N., and Sygusch, J. (1997) *Nat. Struct. Biol.* **4,** 36–39
7. Schoevaart, R., van Rantwijk, F., and Sheldon, R. A. (2001) *J. Org. Chem.* **66,** 4559–4562
8. Hall, D. R., Leonard, G. A., Reed, C. D., Watt, I., Berry, A., and Hunter, W. N. (1999) *J. Mol. Biol.* **287,** 383–394
9. Zgiby, S. M., Thomson, G. J., Qamar, S., and Berry, A. (2000) *Eur. J. Biochem.* **267,** 1858–1868
10. Plater, A., Zgiby, S. M., Thomson, G. J., Qamar, S., Wharton, C. W., and Berry, A. (1999) *J. Mol. Biol.* **285,** 843–855
11. Blom, N., Tetreault, S., Coulombe, R., and Sygusch, J. (1996) *Nat. Struct. Biol.* **3,** 856–862
12. Qamar, S., Marshal, K., and Berry, A. (1996) *Prot. Sci.* **5,** 154–161
13. Cooper, S. J., Leonard, G. A., McSweeney, S. M., Thompson, A. W., Naismith, J. H., Qamar, S., Plater, A., Berry, A., and Hunter, W. N. (1996) *Structure* **4,** 1303–1315
14. Zgiby, S., Plater, A. R., Bates, M. A., Thomson, G. J., and Berry, A. (2002) *J. Mol. Biol.* **315,** 131–140
15. Collins, K. D. (1974) *J. Biol. Chem.* **249,** 136-142
16. Reizer, J., Ramseier, T. M., Reizer, A. Charbit, A., and Saier, M. H. J. (1996) *Microbiology* **142,** 231–250
17. Otwinowski, Z., and Minor, W. (1997) *Methods Enzymol.* **276A,** 307–326
18. Otwinowski, Z. (1991) in *Isomorphous Replacement and Anomalous Scattering, Proceedings of the CCP4 Study Weekend* (Wolf, W., Evans, P. R., and Leslie, A. G. W., eds) pp. 80–86, SERC Daresbury Laboratory, Warrington, UK
19. Cowtan, K. (1994) *Crystallography* **31,** 34–38
20. Collaborative Computational Project Number 4. (1994) *Acta Crystallogr. Sect. D Biol. Crystallogr.* **50,** 760-763
21. Anastassis, P., Morris, R., and Lamzin, V. S. (1999) *Nat. Struct. Biol.* **7,** 458–463
22. Murshodov, G. N., Vagin, A. A., and Dodson, E. J. (1997) *Acta Crystallogr. Sect. D Biol. Crystallogr.* **53,** 240–255
23. Jones, T. A., Zou, J. Y., Cowan, S. W., and Kjeldgaard, M. (1991) *Acta Crystallogr. Sect. A* **47,** 110–119
24. Brünger, A. T., Adams, P. D., Clore, G. M., DeLano, W. L., Gros, P., Grosse-Kunstleve, R. W., Jiang, J. S., Kuszewski, J., Nilges, M., Pannu, N. S., Read, R. J., Rice, L. M., Simonson, T., and Warren, G. L. (1998) *Acta Crystallogr. Sect. D Biol. Crystallogr.* **54,** 905–921
25. Sheldrick, G. M., and Schneider, T. R. (1997) *Methods Enzymol.* **277,** 319–343
26. Morris, G. M., Goodsell, D. S., Halliday, R. S., Huey, R., Hart, W. E., Belew, R. K., and Olson, A. J. (1998) *J. Comput. Chem.* **19,** 1639–1662
27. Goodford, P. J. (1985) *J. Med. Chem.* **28,** 849–857
28. Erion, M. D., and Reddy, M. R. (1998) *J. Am. Chem. Soc.* **120,** 3295–3304
29. van Aalten, D. M., Bywater, R., Findlay, J. B., Hendlich, M., Hooft, R. W., and Vriend, G. (1996) *J. Comput. Aided Mol. Des.* **10,** 255–262
30. Wouters, J. (1998) *Protein Sci.* **7,** 2472–2475
31. Chevrier, B., D'orchymont, H., Schalk, C., Tarnus, C., and Moras, D. (1996) *Eur. J. Biochem.* **237,** 393-398
32. Heine, A., DeSantis, G., Luz, J. G., Mitchell, M., Wong, C.-H., and Wilson, I. A. (2001) *Science* **294,** 369–374
33. Barton, G. J. (1993) *Protein Eng.* **6,** 37–40
34. Kraulis, P. J. (1991) *J. Appl. Crystallogr.* **24,** 946–950
35. Merritt, E. A., and Murphy, M. E. P (1994) *Acta Crystallogr. Sect. D Biol. Crystallogr.* **50,** 869–873